Check for updates

View Article Online
View Journal

Analyst

Accepted Manuscript

This article can be cited before page numbers have been issued, to do this please use: J. Sha, Q. Li, M. Xu, X. Li, S. Li, L. Hou and Y. Chen, *Analyst*, 2020, DOI: 10.1039/D0AN00402B.

This is an Accepted Manuscript, which has been through the Royal Society of Chemistry peer review process and has been accepted for publication.

Accepted Manuscripts are published online shortly after acceptance, before technical editing, formatting and proof reading. Using this free service, authors can make their results available to the community, in citable form, before we publish the edited article. We will replace this Accepted Manuscript with the edited and formatted Advance Article as soon as it is available.

You can find more information about Accepted Manuscripts in the Information for Authors.

Please note that technical editing may introduce minor changes to the text and/or graphics, which may alter content. The journal's standard Terms & Conditions and the Ethical guidelines still apply. In no event shall the Royal Society of Chemistry be held responsible for any errors or omissions in this Accepted Manuscript or any consequences arising from the use of any information it contains.

ROYAL SOCIETY OF CHEMISTRY

rsc.li/analyst

Please do not adjust margins

Journal Name

View Article Online
DOI: 10.1039/D0AN00402B

ARTICLE

Polypyrrole Coating Eightfold Helical Wells-Dawson POMs based Cu-FKZ Framework for Boosting Colorimetric Sensing

Received 00th January 20xx,
Accepted 00th January 20xx

DOI: 10.1039/x0xx00000x
www.rsc.org/

Qian Li,[a,b] Mingqi Xu,[a,b] Xiao Li,[a] Shuxian Li,[b] Liran Hou,[a] Yuhao Chen,[a] Jingquan Sha*[a,b]

To explore novel colorimetric biosensor with highly sensibility and selectivity, a new Wells-Dawson type polyoxometelates (POMs) based metal-organic framework (MOF) with eightfold helix, $[Cu_9(FKZ)_{12}(H_2O)_8][H_3P_2W_{18}O_{62}]_2{\cdot}4H_2O$ ($CuFKZP_2W_{18}$) (HFKZ = 1-(2,4-difluorophenyl)-1,1-bis[(1H-1,2,4-triazol-1-yl)methyl] ethanol), were successfully synthesized, then polypyrrole (PPy) were introduced to fabricate $CuFKZP_2W_{18}$/PPy(n) nanocomposites (n = 7%, 15%, 30%) *via* a facile 'in situ' oxidation polymerization process. All results indicate that $CuFKZP_2W_{18}$/PPy(15%) as the colorimetric biosensor exhibits the lowest limit of detection (0.07 μM towards H_2O_2 and 0.627 μM to ascorbic acid), the smallest K_m value (0.106 mM for H_2O_2 and 0.042 mM for o-phenylenediamine) and the highest sensitivity (0.0227 1/μM towards H_2O_2 and 0.0025 1/μM to ascorbic acid) compared to most reported enzyme mimetics, to the best our knowledge.

Introduction

Natural enzymes have significant practical applications in biosensing due to the high substrate specificities and high efficiency under the mild condition, however, to overcome the challenges associated with the lower stability, sensitivity of catalytic activity in harsh environmental condition, and the higher costs in preparation and purification,[1,2] many artificial enzyme mimetics based on nanomaterials, for example, Fe_3O_4 NPs (nanoparticles),[3] Co_3O_4 NPs,[4] noble metal materials,[5,6] carbon materials (nanotube,[7] dots,[8] and grapheme oxides[9]), polymers,[10] and other nanomaterials,[11,12] have been investigated and exhibited the peroxidase-like catalytic activities. Beyond that, hybrid materials as artificial enzyme mimetics including graphene-,[13] carbon nanotube-,[14] polypyrrole-(PPy-)[15] have been also reported and exhibited better performances owing to the combination and synergistic effect. Although these reported examples as the enzyme mimetics can be potentially used in biosensing and medical diagnosis, further efforts to develop superior colorimetric biosensor with highly sensibility and selectivity are still needed to done in the field of bioinorganic chemistry.

Polyoxometalates (POMs), as a kind of metal oxygen clusters with diverse structures and the excellent redox property, have been widely studied in catalysis, medicine and material science.[16-21] Recently, $XW_{12}O_{40}$ (X= P[22], Si[23]) and tetra-nuclear Zr-substituted POMs[24] have been authenticated good peroxidase-like activities toward H_2O_2 detection by catalytic oxidation of 3,3',5,5'-tetramethylbenzidine (TMB) to form a coloured oxTMB.[25] As we knows, POMs are often introduced into metal-organic frameworks (MOFs) to construct compounds abbreviated as POMOFs, to overcome the inherent shortcomings with their aggregation and small surface areas (<10 m^2g^{-1}).[26-32] More importantly, the accessible ordered porous structure of POMOFs can facilitate substrate diffusion[33,34] and expose more active site[35] at the molecule level, which is conducive to increase the reaction activity. On the other hand, POMOFs with helical features is very interesting because not only living organisms utilize helices to store and transmit genetic information, but also helical compounds have important applications in many important field.[36] We guess that POMOFs with helix maybe a suitable choice for biosensing materials with high structural stability and good biocompatibility. To the best our knowledge, study of Wells-Dawson based POMOFs with helix still remain rare[37-39], especially in the field of biosensor, so the work is highly desired in the field towards enhancing their application-related studies.

Inspired by aforementioned points and comprehensive consideration, Wells-Dawson typed POM precursors were screened to assemble with low-cost Cu metal and fluconazole (FKZ) molecules, so as to directly obtain Wells-Dawson based POMOFs with helix for the following reasons: (a) 54 coordination oxygen atoms of Wells-Dawson offer more flexible potential sites resulting in the covalent graft with ease. (b) FKZ molecule contains N-/O-mixed donors and possess better flexibility, facilitating the realization of helical structure. (c) FKZ as one kind of antifungal medicine can endow unexpected properties of targeted compounds. As expected, a new Wells-Dawson based POMOF compound containing eightfold helix, $[Cu_9(FKZ)_{12}(H_2O)_8][H_3P_2W_{18}O_{62}]_2{\cdot}4H_2O$ ($CuFKZP_2W_{18}$), were successfully isolated, then employed as an efficient and stable colorimetric sensor towards H_2O_2 and ascorbic acid (AA) detection. Although practical results of $CuFKZP_2W_{18}$ as enzyme mimetics show the improved peroxidase-like mimicking

[a] Department of Chemistry and Chemical Engineering, Jining University, Qufu, Shandong 273155, P. R.China.
[b] School of Pharmacy, Jiamusi University, HeilongJiang, Jiamusi, 154007, P.R. China
E-mail: shajq2002@126.com.
Electronic Supplementary Information (ESI) available: additional Figures and Tables. See DOI: 10.1039/x0xx00000x

Published on 14 April 2020. Downloaded by University of Birmingham on 4/14/2020 9:32:33 AM.

Analyst Accepted Manuscript

Please do not adjust margins

View Article Online DOI: 10.1039/D0AN00403B

Published on 14 April 2020. Downloaded by University of Birmingham on 4/14/2020 9:32:33 AM.

activities due to the synergistic effect of all components, the poor conductivity results in the relatively low value. Fortunately, fabrication of POMOFs into composite with carbon materials with good conductivity can significantly enhance their catalytic performances.[40,41] As a consequence, $CuFKZP_2W_{18}$ was coated with polypyrrole (PPy) to fabricate nanocomposites named as $CuFKZP_2W_{18}$/PPy(n) (n = 7%, 15%, 30%), which shows excellent peroxidase-like catalytic activity towards H_2O_2 and AA detection compared with reported artificial enzyme mimetics.

Experimental Section

Materials and methods

All reagents were of analytical grade and used without purification, and human serum samples were purchased from Hongquan Biotechnology Co., Ltd. (Guangzhou, China). Elemental analyses (C, H, and N) were performed on a PerkinElmer 2400 CHN analyzer. The structural characterization was performed by IR spectra on an Alpha Centaurt FT/IR spectrometer with KBr pellets from 400 to 4000 cm^{-1}, and X-ray photoelectron spectroscopy (XPS) on a scanning X-ray microprobe (K-Alpha, Thermo Scientific) with Al kα radiation. The phase characterization was performed by powder X-ray diffraction (PXRD) pattern on the Rigaku Dmax 2000 X-ray diffractometer with Cu-Kα radiation and 2θ ranging from 5° to 50°. The morphology was characterized by scanning electron microscopy (SEM) and energy dispersive spectroscopy (EDS) spectroscopy on a Phenom ProX scanning electron microscope. All the reactions were recorded on UV-vis spectroscopy (Hitachi UV2010 spectrophotometer) at 422 nm.

Synthesis of $[Cu_9(FKZ)_{12}(H_2O)_8][H_3P_2W_{18}O_{62}]_2{\cdot}4H_2O$ ($CuFKZP_2W_{18}$)

A mixture of $Cu(NO_3)_2$ (0.150 g, 0.80 mmol), HFKZ (0.080 g, 0.57 mmol), NH_4VO_3 (0.036 g, 0.31 mmol) and $K_6P_2W_{18}O_{62}$ (0.300 g, 0.07 mmol) was dissolved in 8 mL water. After pH of the mixture was adjusted to 3.00 with 1 M HCl and stirred for 30 min, the resulting solution was transferred into a 23 mL Teflon-lined autoclave and heated at 170 °C for 5 days. After cooling to room temperature slowly, green block crystals were obtained and washed with distilled water and air-dried (yield: 41% based on W). Elemental analysis: $C_{156}H_{174}Cu_9F_{24}N_{72}O_{148}P_4W_{36}$ (13195.45). Anal. Calcd: H, 1.319; C, 14.187; N, 7.639 (%). Found: H, 1.643; C, 14.179; N, 7.634 (%).

X-ray crystallographic study of $CuFKZP_2W_{18}$

Single crystal X-ray diffraction (SCXRD) data for $CuFKZP_2W_{18}$ were recorded on a Bruker SMART-CCD diffractometer with Mo-Kα radiation (λ = 0.71073 Å) at 296 K. The structure was solved by direct methods and refined by full-matrix last squares on F^2 through the SHELXTL and WINGX software package.[42] Semiempirical absorption corrections were applied using the SADABS program. All non-hydrogen atoms were refined anisotropically and the positions of hydrogens on carbons were calculated theoretically. The detailed crystal data and structure refinements are summarized in Table 1. Selected bond lengths and angles are listed in Table S1. Crystallographic data have been deposited with CCDC number 1940345.

Preparation of nano-$CuFKZP_2W_{18}$

Crystals $CuFKZP_2W_{18}$ were ground for 5 h with an agate mortar and pestle, and the resulted powder was dissolved in methanol and placed in a microwave digestion tank, then heated in a microwave oven at 400 W for 6 h. The suspension of $CuFKZP_2W_{18}$ was separated by centrifugation, rinsed with water and ethanol, and then dried in a vacuum drier at 80 °C for 24 h.

Table 1. Crystal data and structure refinements for $CuFKZP_2W_{18}$.

Chemical formula	$C_{156}H_{174}Cu_9F_{24}N_{72}O_{148}P_4W_{36}$
Formula weight	13195.45
CCDC	1940345
Temperature (K)	296(2)
Wavelength (Å)	0.71073
Crystal system	Monoclinic
Space group	*P 21/n*
a (Å)	15.3689(17)
b (Å)	34.520(4)
c (Å)	28.618(3)
α (°)	90
β (°)	99.017(2)
γ (°)	90
V (Å^3)/Z	14995(3)/4
Density (g·cm^{-3})	2.884
Abs coeff. (mm^{-1})	14.500
F(000)	11650
Data collect θ range	1.382 to 25.000
Collected/ Independent Reflns	75328/26396
R_{int}	0.0497
Data/restraints/parameters	26386/60/1821
Goodness-of-fit on F^2	1.048
Final R indices [I > 2δ(I)]	R_1 = 0.0499, wR_2 = 0.1278
R indices (all data)	R_1 = 0.0822, wR_2 = 0.1484
Largest diff. peak and hole (e.Å^{-3})	4.613 and -2.496

$R_1 = \Sigma(||F_0|-|F_c||)/\Sigma|F_0|$, $wR_2 = \Sigma w(|F_0|^2-|F_c|^2)^2/\Sigma w(|F_0|^2)^2]^{1/2}$

Preparation of PPy and PPy coating $CuFKZP_2W_{18}$

$CuFKZP_2W_{18}$ (0.050 g, 3.8×10^{-6} mol) was dissolved in 10 mL deionized water in a beaker. Then, pyrrole (7.5 μL, 1.08×10^{-4} mol) was dissolved in 2 mL ethanol and placed in the above solution. Next, 10 mL $FeCl_3$ solution (0.050 g, 3.1×10^{-4} mol) as the catalyst was slowly added to the mixture. After the mixture was stirred in ice bath for 10 h and then held for 12 h, the black precipitate was separated, washed, and dried in an oven at 60 °C for 24 hours, named as $CuFKZP_2W_{18}$/PPy(15%). Meanwhile, in order to compare the performances of composites with different loading amount of pyrrole, a series of composites were synthesized, and were abbreviated as $CuFKZP_2W_{18}$/PPy(n) ("n" value is the percentage content of pyrrole to the total mass used in the synthesis process, here 7%, 15% and 30% are used). PPy was obtained using a similar method to that of $CuFKZP_2W_{18}$/PPy(n), but no $CuFKZP_2W_{18}$.

Peroxidase-like activity of $CuFKZP_2W_{18}$ and $CuFKZP_2W_{18}$/PPy(n)

Herein, the catalytic oxidation of o-phenylenediamine (OPD) was tested in the presence of H_2O_2 in order to evaluate the peroxidase-like activity of $CuFKZP_2W_{18}$ and $CuFKZP_2W_{18}$/PPy(n). More specifically the absorbance change of OPD on a UV-vis spectrophotometer at 422 nm was monitored, and reaction conditions: 0.6 mg/mL catalyst ($CuFKZP_2W_{18}$, $CuFKZP_2W_{18}$/PPy(n), PPy), 30 μM OPD and 100 μM H_2O_2 as substrate in the acetate buffer solution (pH=7.0) at 40 °C for 4 min. The influence of pH value ranging from 4.5 to 8.0 and temperature from 25°C to 60 °C on the activity were investigated. Moreover, the steady-state

Analyst Accepted Manuscript

 This journal is © The Royal Society of Chemistry 20xx

View Article Online
DOI: 10.1039/D0AN00408B

Published on 14 April 2020. Downloaded by University of Birmingham on 4/14/2020 9:32:33 AM.

kinetics measurements were carried out in time course mode by varying the concentrations of one and fixing the concentrations of another. Finally, the mixed solution are incubated at 40 °C for standard curve measurement.

The Michaelis-Menten constant was calculated using the Lineweaver-Burk plots of the double reciprocal of the Michaelis-Menten equation,

$$v=V_{max}\times[S]/(K_m+[S])$$

where v is the initial velocity, V_{max} represents the maximum reaction velocity, [S] is the concentration of the substrate and K_m is the Michaelis constant.

H_2O_2 and AA Detection Assay

H_2O_2 content can be detected according to the standard curve of H_2O_2. And the AA detection was performed as follows. OPD (30 μM), H_2O_2 (100 μM), catalyst (0.6 mg/mL), and different amount of AA were added into the acetate buffer solution (pH=7.0) in turn, then the mixture solutions were shaken and equilibrated for 4 min and filtered using a syringe filter immediately. The oxOPD content was tested through UV spectra at 422 nm.

Several potential interfering substance, glucose (Glu) and 5 kinds of ions (Mg^{2+}, Na^+, K^+, NO_3^- and Cl^- (240 μM)) were added to the OPD-catalyst-H_2O_2 system. In addition, the serum samples were treated by centrifugation (12 000 rpm, 30 min) to obtain the supernatants for the next-step measurement in order to assess the AA determination in real samples.

Results and discussion

Structural description of $CuFKZP_2W_{18}$

Single-crystal structure analysis reveals that $CuFKZP_2W_{18}$ crystallizes in the monoclinic space group *P 21/n* and consists of two independent $[P_2W_{18}O_{62}]^{6-}$ polyoxoanions (abbreviate to P_2W_{18}), nine Cu ions, twelve FKZ molecules, and twelve water (Figure S1a, SI). There are five crystallography independent Cu ions (Cu1, Cu2, Cu3, Cu4, Cu5), and their coordination modes are illustrated in Figure S1b (SI), in which Cu4 and Cu5 connect each other through oxygen atoms of H_2O molecule. And there are two crystallography independent FKZ molecules (FKZ-1 and FKZ-2), in which FKZ-1 connect with two Cu ions (Cu1 and Cu2), and FKZ-2 connect with four Cu ions (two Cu4 and two Cu5) giving a tetradentate linking mode (Figure S1c, SI). As a consequence, each P_2W_{18} linking with seven Cu ions (Cu1, Cu2, 2Cu3, Cu4, 2Cu5) extend and dominate the formation of $CuFKZP_2W_{18}$ (Figure S1d, SI). The bond lengths are in the range of 1.940-2.038 Å for Cu-N bonds and 1.900-2.860 Å for Cu-O bonds (Table S2, SI). On basis of the combined results of X-ray single-crystal structure analysis, elemental analysis, bond-valence sum, the X-ray photoelectron spectroscopy (XPS) and the crystal colour, the formula was determined to be $[Cu_9(FKZ)_{12}(H_2O)_8][H_3P_2W_{18}O_{62}]_2\cdot 4H_2O$.

Due to the nature of P_2W_{18} and FKZ molecules, compound $CuFKZP_2W_{18}$ exhibits a complicated three-dimensional framework. More concretely, taking no account of FKZ ligands, P_2W_{18} polyoxoanions link with Cu1, Cu3, Cu4 and Cu5 forming a three-dimensional inorganic backbone (Figure S2a, SI) containing one type of meso-helices. Namely, P_2W_{18} and Cu ions connect each other along the same route of {-P_2W_{18}-Cu3-P_2W_{18}-Cu5/Cu4-P_2W_{18}-Cu3-P_2W_{18}-Cu1-}$_n$ constructing the left- and right-handed helices (named Type-I), shown in Figure 1a. Then the left- and right-handed helices with the same thread pitch of 15.3689 Å are connected together by sharing P_2W_{18} polyoxoanions and Cu3 obtaining a one dimensional double channels. On the other hand, taking no account of P_2W_{18} polyoxoanions, FKZ ligands with Cu1, Cu2, and Cu3 also fabricate a three-dimensional organic-inorganic hybrid backbone (Figure S2b, SI), further evolving into the Type-II twofold meso-helixes (Figure 1b). The left-handed helix is completed along the route of {-Cu2-FKZ-Cu3-FKZ-Cu1-FKZ-Cu2-}$_n$, and the right-handed helix is obeyed the opposite route. Both have an identical thread pitch of 15.3689 Å. Finally, from an overall perspective, Type-I and Type-II arrays connect together *via* sharing the FKZ-2 generating the whole three-dimensional framework of $CuFKZP_2W_{18}$ in Figure S2c (SI). To clarity the complex structure, the whole framework can be simplified as a 4,5,6,8-net with the point symbol of $\{3\cdot4^4\cdot5\cdot6^4\}^2$ $\{3^2\cdot4^4\cdot5^4\cdot6^2\cdot7^3\}$ $\{3^2\cdot4^6\cdot5^4\cdot6^8\cdot7^6\cdot8^2\}\{4^2\cdot6^3\cdot7\}^2$, in which the Cu1, Cu2, Cu3 as 4-, 5-, 6-connected nodes, and P_2W_{18} as 8-connected nodes. (Figure S2d, SI)

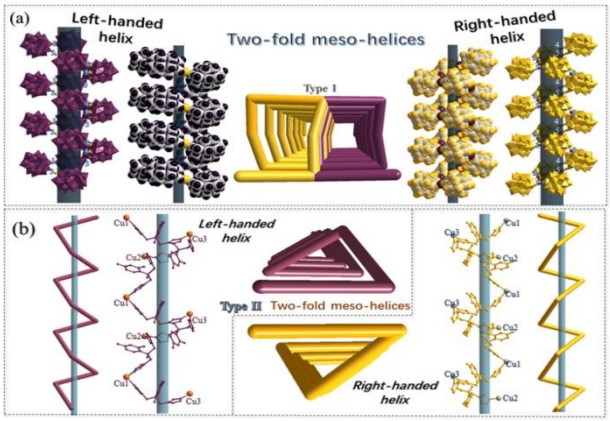

Fig. 1 (a) Polyhedral and space-filling representation of the Type-I meso-helixes constructed by Cu-POMs (P_2W_{18}, Cu1, Cu3, Cu4 and Cu5) along *a* axis. (b) Ball/stick representation and topology of Type-II meso-helixes constructed by Cu-MOFs (Cu1, Cu2, Cu3, Cu5 and FKZ-1) along *a* axis.

Excitingly, two other types of helical chain can be obsreved in the whole framework. More specifically, Cu2 links with P_2W_{18} directly and Cu3 *via* FKZ-1 construct the Type-III helices with the thread pitch of 15.3689 Å, in which the left- and right-handed helices are in the same route of {Cu2-P_2W_{18}-Cu3-Cu2-P_2W_{18}}$_n$ (Figure 2a). Moreover, two P_2W_{18} clusters can be connected together *via* different Cu ions forming three different kinds of dimer (Figure 2b), then three kinds of dimer are alternately linked together through FKZ-1 and Cu2, giving birth to Type-IV helices. The left-handed helix is along the route of {subunit A-Cu2-subunit B-Cu2-subunit C}$_n$, and the right-handed helix is obeyed the opposite route (Figure 2c). Besides, there is another interesting structural feature, namely, a pseudo cage like a bowl-shaped capsule is constructed by Cu ions (Cu1, Cu2, 2Cu3, 2Cu5), P_2W_{18} polyoxoanions and FKZ ligands, in which P_2W_{18} clusters are in the center(Figure 2d).

Analyst Accepted Manuscript

View Article Online
DOI: 10.1039/D0AN00402B

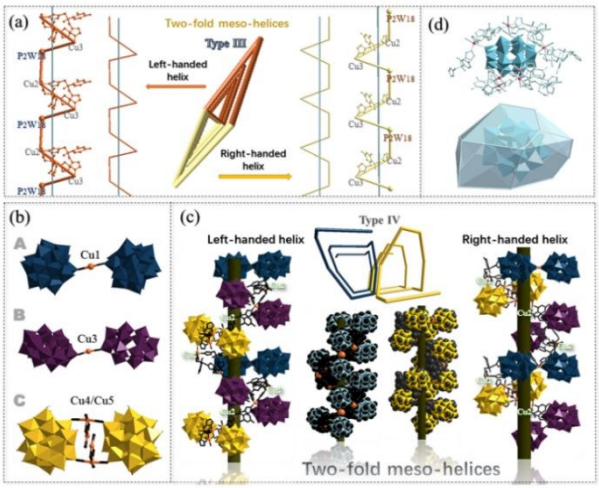

Fig. 2. Ball/stick/polyhedral/space-filling/topology representation of Type-III twofold meso-helixes constructed by P_2W_{18}, Cu2, Cu3 and FKZ-1 along *a* axis (a), three different types of dimeric structures (b), Type-IV twofold meso-helixes constructed by dimeric structures, Cu2, FKZ-1 and FKZ-2 along *a* axis (c), a pseudo cage like a bowl-shaped capsule constructed by Cu and FKZ covering the P_2W_{18} clusters (d).

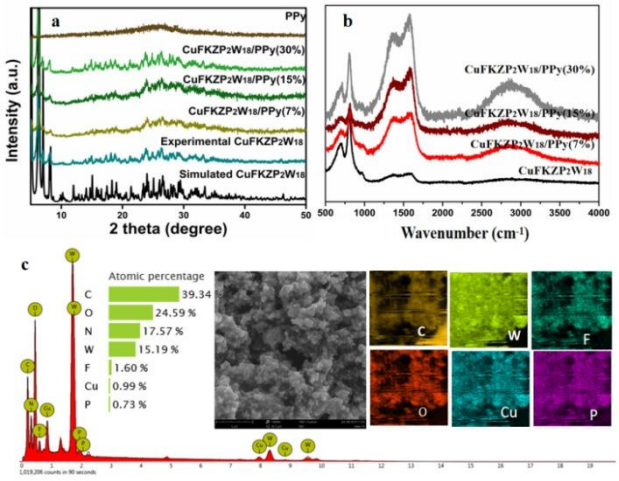

Fig. 3 (a) PXRD patterns and (b) Raman spectra of $CuFKZP_2W_{18}$, $CuFKZP_2W_{18}$/PPy (n); (c) EDS, SEM and elemental mapping images of $CuFKZP_2W_{18}$/PPy(15%).

PXRD, IR, Raman, XPS, SEM and EDS Analyses

The phase purity of $CuFKZP_2W_{18}$ was certified by PXRD measurement, in which the experimental pattern is in good agreement with the simulated one, indicating that the collected samples are pure (Figure S3a, SI). PXRD patterns of $CuFKZP_2W_{18}$/PPy (n) is similar to that of $CuFKZP_2W_{18}$, testifying that the structure of $CuFKZP_2W_{18}$ does not collapse during the polymerization of Py (Figure 3a). Characteristic bands in FT-IR spectra at 1077, 960, 910 and 780 cm^{-1} for $CuFKZP_2W_{18}$ are attributed to ν (P-O), ν (W=O_d), ν (W-O_b-W), and ν (W-O_v-W) vibrations (Figures S3b, SI). And the peaks of $CuFKZP_2W_{18}$/PPy (n) are similar to that of matrix $CuFKZP_2W_{18}$ (Figures S4, SI). In addition, compound $CuFKZP_2W_{18}$ is also stable in aqueous solutions in the pH range of 3-10 for 12 hours at room temperature, confirmed by PXRD and IR measurements (Figure S5, SI), which is benefit for practical applications of $CuFKZP_2W_{18}$ as catalysts. Raman spectra of $CuFKZP_2W_{18}$/PPy(n) (λ = 532 nm) present characteristic bands of PPy at 1345 cm^{-1} and 1579 cm^{-1} attributed to the C-N and C=C stretching,[43,44] indicating the successful fabrication of $CuFKZP_2W_{18}$/PPy(n) composite materials (Figure 3b and S6). Moreover, in order to further verify the pyrrole loading on the surface of $CuFKZP_2W_{18}$, the morphologies of $CuFKZP_2W_{18}$ and $CuFKZP_2W_{18}$/PPy(15%) composite were investigated with scanning electron microscope (SEM) and the homogenous distribution of elements with EDS and the mapping images (Figures 3c and S7, SI). It can be clearly observed that $CuFKZP_2W_{18}$/PPy(15%) composite shows a coarse and circular fringe due to the wrapping of PPy, meanwhile the EDS and elemental mapping images indicate the presence and the homogenous distribution of C, O, W, P, F, Cu and N elements in $CuFKZP_2W_{18}$ and $CuFKZP_2W_{18}$/PPy(15%), respectively.

Compositions and oxidation states of $CuFKZP_2W_{18}$ and $CuFKZP_2W_{18}$/PPy(15%) were further evaluated by the X-ray photoelectron spectroscopy (XPS) shown in Figure 4. The XPS spectra survey of both $CuFKZP_2W_{18}$ and $CuFKZP_2W_{18}$/PPy(15%) have showed the co-existence of C, O, N, W, P, F, and Cu elements clearly, indicating the presence of $CuFKZP_2W_{18}$ in $CuFKZP_2W_{18}$/PPy(15%) (Figure 4a). Two peaks at 37.7 eV and 35.5 eV can be attributed to W^{6+} $4f_{5/2}$ and W^{6+} $4f_{7/2}$, respectively (Figure 4b), and three Gaussian peaks at 284.6 eV, 285.3 eV and 286.5 eV can be ascribed to C-C/C=C, C-O, and C-N/C=N, respectively in $CuFKZP_2W_{18}$ and $CuFKZP_2W_{18}$/PPy(15%) (Figure 4c). Moreover, the peak position of O 1s spectra show the transfer from 530.6 eV in $CuFKZP_2W_{18}$ to 531.8 eV in $CuFKZP_2W_{18}$/PPy(15%) (Figure S8, SI). All the results mentioned above indicate the stabilization of $CuFKZP_2W_{18}$ and the introduction of PPy in $CuFKZP_2W_{18}$/PPy(15%) successfully. More importantly, the N 1s spectra of $CuFKZP_2W_{18}$/PPy(15%) shows two peaks at 399.7 eV and 400.4 eV belonging to -NH- and $-NH^+$- in PPy, while another peak at 401.3 eV can be ascribed to -N= in FKZ ligand, confirming the stabilization of $CuFKZP_2W_{18}$ framework and the fabrication of PPy successfully again (Figure 4d).

Published on 14 April 2020. Downloaded by University of Birmingham on 4/14/2020 9:32:33 AM.

Analyst Accepted Manuscript

This journal is © The Royal Society of Chemistry 20xx

View Article Online
DOI: 10.1039/D0AN00402B

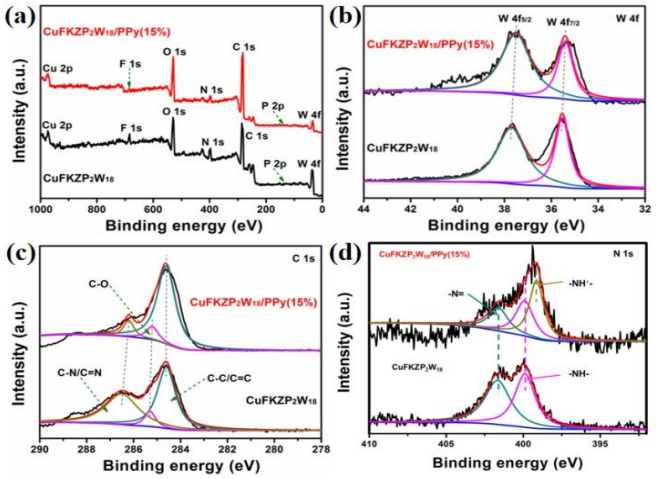

Fig. 4. XPS spectra of CuFKZP$_2$W$_{18}$ and CuFKZP$_2$W$_{18}$/PPy(15%): (a) survey, (b) W 4f, (c) C 1s, and (d) N 1s.

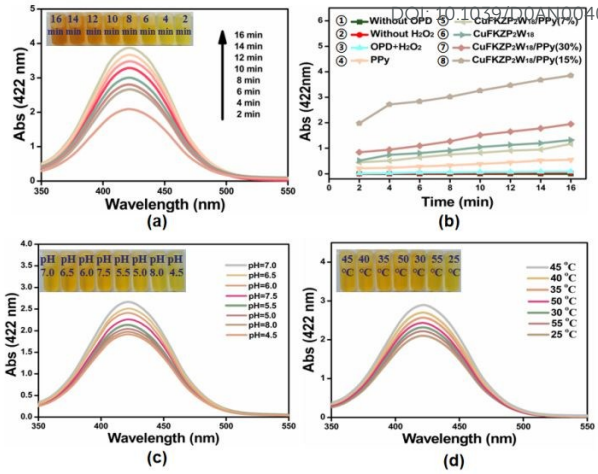

Fig. 5. (a) UV-vis absorption spectra of CuFKZP$_2$W$_{18}$/PPy(15%)-catalyzed OPD colorimetric system as a function of reaction time from 2 to 16 min; (b) Time-dependent absorbance of control experiments at 422 nm under typical conditions: ① CuFKZP$_2$W$_{18}$/PPy(15%) + H_2O_2; ② CuFKZP$_2$W$_{18}$/PPy(15%) + OPD; ③ H_2O_2 + OPD; ④ PPy + H_2O_2 + OPD; ⑤ CuFKZP$_2$W$_{18}$/PPy(7%) + H_2O_2 +OPD; ⑥ CuFKZP$_2$W$_{18}$ + H_2O_2 + OPD; ⑦ CuFKZP$_2$W$_{18}$/PPy(30%) +H_2O_2 +OPD; ⑧ CuFKZP$_2$W$_{18}$/PPy(15%)+H_2O_2+OPD (the inset shows the corresponding photographs). (c and d) Dependence of the peroxidase-like activity of CuFKZP$_2$W$_{18}$/PPy(15%) on the different pH and temperature under typical conditions (pH value: 4.5, 5.0, 5.5, 6.0, 6.5, 7.0, 7.5, 8.0; T: 25, 30, 35, 40, 45, 50, 55 °C). Typical reaction conditions: in the acetate buffer solution (pH=7), catalyst 0.6 mg/mL, catalyst 0.6 mg/mL, H_2O_2 100 μM, OPD 30 μM, time 4 min and temperature 40 °C.

CuFKZP$_2$W$_{18}$/PPy(n) rapidly catalyze oxidation of OPD

POMs and POMs based composites have been confirmed to possess the satisfactory peroxidase-like activity,[45] so the peroxidase-like activities of CuFKZP$_2$W$_{18}$ and CuFKZP$_2$W$_{18}$/PPy(n) were investigated by the catalytic oxidation of peroxidase substrate OPD in the attendance of H_2O_2 (Scheme S1, SI). As shown in Figure 5a, a remarkable absorption peak at ca. 422 nm and obvious yellow for oxOPD could be observed in the presence of CuFKZP$_2$W$_{18}$/PPy (15%), indicating the CuFKZP$_2$W$_{18}$/PPy (15%) nanocomposite can trigger the oxidization of OPD. To examine the catalytic activity, a series of control experiments were tested shown in Figure 5b. More specifically, no colour change can be observed (curves ① and ②), indicating that no oxidation reaction occurs in the absence of CuFKZP$_2$W$_{18}$/PPy(15%) (Figures S9, SI). Moreover, a solution containing only OPD or H_2O_2 failed to obtain a yellow coloured solution (curve ③). Both demonstrate that CuFKZP$_2$W$_{18}$/PPy(15%) possesses a peroxidase-like catalytic ability and can thus catalyze the oxidation of OPD by H_2O_2. Meanwhile, to investigate the effect of PPy on CuFKZP$_2$W$_{18}$, the peroxidase-like catalytic activities of CuFKZP$_2$W$_{18}$, PPy and CuFKZP$_2$W$_{18}$/PPy (7% and 30%) were also investigated under the same conditions as that of CuFKZP$_2$W$_{18}$/PPy(15%) (Figures 5b and S10, SI), and the results show that different intensities of absorption peaks and colour could be observed (curves ④-⑧), and the absorption peak intensities decrease in the following order: CuFKZP$_2$W$_{18}$/PPy(15%)>CuFKZP$_2$W$_{18}$/PPy(30%)>CuFKZP$_2$W$_{18}$>CuFKZP$_2$W$_{18}$/PPy(7%)>PPy. The fact can be deduced preliminarily as follows: (1) CuFKZP$_2$W$_{18}$ and CuFKZP$_2$W$_{18}$/PPy(n) possess peroxidase-like activities due to excellent redox of P$_2$W$_{18}$ and the electrostatic interactions/hydrogen bonds/π-π stacking among OPD with FKZ and/or PPy. (2) The peroxidase-like activity of CuFKZP$_2$W$_{18}$/PPy(15%) is highest, indicating that the peroxidase-like activity of CuFKZP$_2$W$_{18}$/PPy(n) depend on the synergistic effect from the integration of all components. (3) Except for the enhancing conductivity, large surface area, the adsorption capacity of PPy to substrate, strong interactions between PPy and CuFKZP$_2$W$_{18}$ may significantly alter the redox properties of CuFKZP$_2$W$_{18}$ toward the oxidation of OPD. Therefore, CuFKZP$_2$W$_{18}$/PPy(15%) composite was used to perform the following peroxidase-like activity evaluation.

To clarify whether the nature of CuFKZP$_2$W$_{18}$/PPy(15%) catalytic oxidation of OPD originate from the generation of the hydroxyl radical (•OH) from the decomposition of H_2O_2 or not, the fluorescence spectrum was employed by using terephthalic acid (TA) (Figure S11, SI and Scheme S2, SI). The result shows that the fluorescence intensity of TA in the presence of CuFKZP$_2$W$_{18}$/PPy(15%) was 8 times higher than that in the absence of CuFKZP$_2$W$_{18}$/PPy(15%), suggesting that •OH is generated.

Optimization of experimental conditions

Similar to natural peroxidase enzyme, the catalytic activity of CuFKZP$_2$W$_{18}$/PPy(15%) was dependent on pH value, temperature, dosage of nanocomposite. As shown in Figures 5c, 5d, S12 and S13 (SI), the optimal pH value (4.5, 5.0, 5.5, 6.0, 6.5, 7.0, 7.5, 8.0) and temperature (25, 30, 35, 40, 45, 50, 55 °C) are 7.0 and 45 °C, respectively. And the dosage effect on the peroxidase-like activity was also explored, and relative activities increase with the increasing dosage from 0.1 to 0.6 mg/mL, then decrease with the increasing dosage from 0.6 to 0.8 mg/mL. Considering that CuFKZP$_2$W$_{18}$/PPy(15%) also exhibits good catalytic activity at 40 °C, which is closer to the physiological temperature of human body, so 40 °C was used as the best reaction temperature. As a result, pH 7.0, temperature 40 °C and dosage 0.6 mg/mL were chosen as the optimized condition for the following assay.

Steady-state kinetic assay and catalytic mechanism of CuFKZP$_2$W$_{18}$/PPy(15%)

The Michaelis-Menten equation was used to analyzed the kinetics of an enzymatic reaction, in which K_m is an index of enzyme affinity to substrate, and a smaller value of K_m represents the stronger enzyme affinity (CuFKZP$_2$W$_{18}$/PPy(15%)) to substrate (OPD and

Published on 14 April 2020. Downloaded by University of Birmingham on 4/14/2020 9:32:33 AM.

Analyst Accepted Manuscript

View Article Online
DOI: 10.1039/D0AN00402B

Published on 14 April 2020. Downloaded by University of Birmingham on 4/14/2020 9:32:33 AM.

H_2O_2). As shown in Figures 6a, 6b and S14 (SI), the K_m value of $CuFKZP_2W_{18}$/PPy(15%) as catalyst are 0.106 mM for H_2O_2 and 0.042 mM for OPD, which is lower than that of $CuFKZP_2W_{18}$ (0.187 mM for H_2O_2, 0.063 Mm for OPD) and other reported enzyme mimics (table 2), meaning that the peroxidase-like activities of $CuFKZP_2W_{18}$ and its composites are superior to other reported compounds, maybe due to the faster electron transfer and the more chance of substrates (H_2O_2 and OPD) to active centers provided by coexistence of the four types of helices. Meanwhile, V_{max} value of $CuFKZP_2W_{18}$/PPy(15%) as catalyst (6.73×10^{-8} M s^{-1} for H_2O_2, 5.49×10^{-8} M s^{-1} for OPD) is also higher than that of $CuFKZP_2W_{18}$ (4.25×10^{-8} M s^{-1} for H_2O_2, 4.18×10^{-8} M s^{-1} for OPD) and other reported enzyme mimics (table 2). The facts fully confirms that $CuFKZP_2W_{18}$/PPy(15%) possesses higher binding affinity with H_2O_2 and OPD. According to the previous report,[46] due to the larger surface area, the adsorption capacity of PPy to substrate is more obvious than other substances, which is consistent with the enhancing peroxidase-like activity of $CuFKZP_2W_{18}$/PPy(15%).

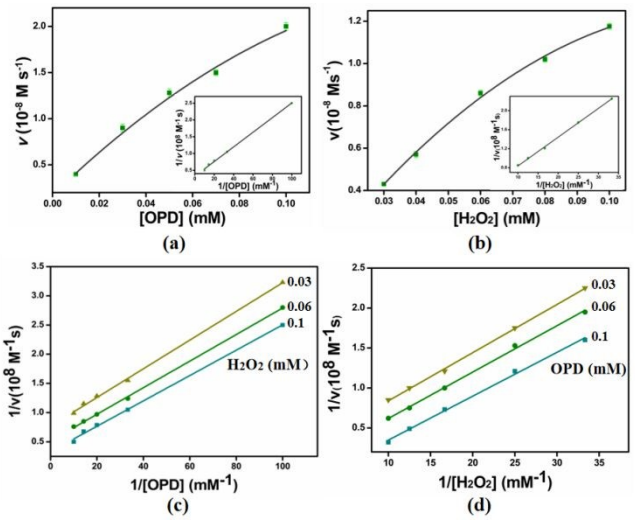

Fig. 6. (a) Steady-state kinetic assays of $CuFKZP_2W_{18}$/PPy(15%): (a) 100 μM H_2O_2 with varying OPD concentration, (b) 30 μM OPD with varying H_2O_2 concentration. (c and d) Double reciprocal plots of the activity of $CuFKZP_2W_{18}$/PPy(15%) with the concentration of H_2O_2 (0.03 mM; 0.06 mM; 0.1 mM) fixed and OPD fixed (0.03 mM; 0.06 mM; 0.1 mM). The reactions were performed in pH=7.0 buffer solution with $CuFKZP_2W_{18}$/PPy(15%) (0.6 mg/mL) 4 min at 40 °C.

Table 2. K_m and V_{max} of $CuFKZP_2W_{18}$, $CuFKZP_2W_{18}$/PPy(15%), and other reported enzyme mimics.

Enzyme mimics	H_2O_2		OPD		Ref.
	K_m (mM)	V_{max} (10^{-8}M s^{-1})	K_m (mM)	V_{max} (10^{-8}M s^{-1})	
HRP	0.34	9.48	0.59	4.65	[47]
MnO_2	0.12	5.71	0.31	8.21	[48]
BiW_9Cu_3	0.29	0.69	——	——	[49]
SbW_9Cu_3	0.25	0.71	——	——	[49]
MOF(Co/2Fe)	4.22	4.91	——	——	[50]
Fe-MIL-88NH_2	0.206	7.04	——	——	[51]
MIL-53(Fe)	0.04	1.86	——	——	[52]
$CuFKZP_2W_{18}$	0.187	4.25	0.063	4.18	*
$CuFKZP_2W_{18}$ /PPy(15%)	0.106	6.73	0.042	5.49	*

*= this work

The double reciprocal plots of the initial velocity against H_2O_2 (OPD) concentration were obtained over a range of OPD (H_2O_2) concentrations shown in Figures 6c and 6d. The almost parallel lines indicate that the catalytic reaction follows the ping-pong mechanism similar to natural enmzy,[53] more concretely, $CuFKZP_2W_{18}$/PPy(15%) binds and reacts with the first substrate, then releases the first product before reacting with the second substrate.

Detection of H_2O_2 and AA

Given the peroxidase-like properties of $CuFKZP_2W_{18}$/PPy(15%), the colorimetric method for quantitative detecting H_2O_2 were established. As shown in Figure 7a and b, the absorbance intensity increases with the increasing H_2O_2 concentration from 5 to 1000 μM, and the absorbance (422 nm) is proportional to H_2O_2 concentration ranging from 5 to 100 μM with the limit of detection (LOD) of 0.07 μM (LOD=KS_0/S), which is lower than that of Fe_3O_4 MNPs (0.5 μM), CeO_2/TiO_2 (3.2 μM) and other reported peroxidase mimics, implying the superiority as the H_2O_2 detector. And the sensitivity is estimated to be 0.0227 1/μM, higher than other colorimetric sensors for H_2O_2, eg. Cu-fkz (0.007 1/μM) and CeO_2/TiO_2 (0.9257×10^{-3}) (Table 3). More importantly, the color change is also easy to observe, meaning a simple and easy method for the naked eye detection of low concentration H_2O_2.

Because AA can efficiently reduce and induce $CuFKZP_2W_{18}$/PPy(15%) to restore oxOPD to OPD, AA can be also detected quantitatively by $CuFKZP_2W_{18}$/PPy(15%) based colorimetric biosensor. More specifically, the absorbance intensity fade with the increasing AA concentration in the range of 5-1000 μM, and the typical concentration-response curves of AA show good linear correlation with the absorption intensity ranging from 5 to 100 μM (Figure 7c and d). The linear regression equation could be expressed as $\Delta A=0.0025C_{AA}+2.2170$ ($R^2=0.997$). The LOD was estimated to be 0.627 μM, which is lower than other AA colorimetric sensor, eg. CuNPs/C (1.41 μM) and $AgFKZSiW_{12}$/PPy (2.7 μM).

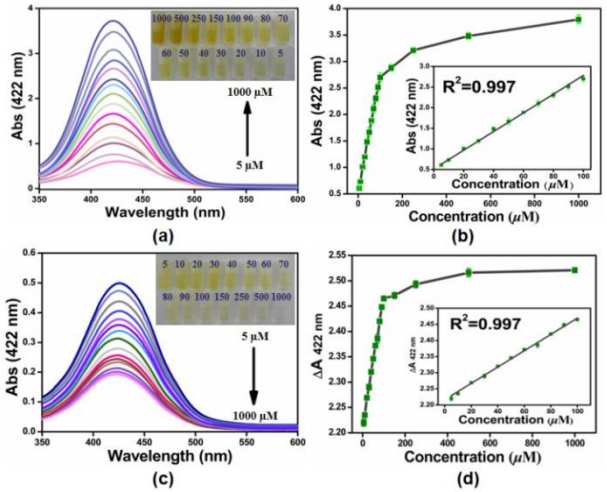

Fig. 7. (a) UV-vis spectra of OPD oxidation catalyzed by $CuFKZP_2W_{18}$/PPy(15%) (0.6 mg/mL) with various H_2O_2 concentrations and (b) concentration-response curve and corresponding linear calibration plot for H_2O_2 detection in buffer solution (pH=7.0). (c) UV-vis spectra of OPD oxidation catalyzed by $CuFKZP_2W_{18}$/PPy(15%) with various AA concentrations as an inhibitor and (d)

Analyst Accepted Manuscript

This journal is © The Royal Society of Chemistry 20xx

concentration-response curve and corresponding linear calibration plot for AA detection in buffer solution (pH=7.0). $\Delta A=A_0-A_i$ (A_0 and A_i are the absorbance at 422 nm before and after the addition of AA with a concentration of i, respectively). Typical reaction conditions: acetate buffer solution (pH=7), H_2O_2 100 μM, AA 80 μM, OPD 30 μM and 4 min at 40 °C.

Table 3. Comparison of the sensing parameters among various nanozymes for their colorimetric sensing of H_2O_2 and AA.

Enzyme mimics	Analyte	LOD (μM)	Range (μM)	Sensitivity (1/μM)	Ref.
Fe^{3+} ions	H_2O_2	0.97	1-100	——	[54]
$FeHPO_4$	H_2O_2	1	57-525	286	[55]
P-Co_3O_4	H_2O_2	0.77	1-30	——	[56]
AuNPs	H_2O_2	0.5	2-200	1.604	[57]
V_2O_5	H_2O_2	1	1-500	——	[58]
CeO_2/TiO_2	H_2O_2	3.2	5-100	925.7	[59]
MOF-808	H_2O_2	4.5	10-1000	0.003	[60]
$AgFKZSiW_{12}$ /PPy	H_2O_2	0.12	1-100	0.0154	[61]
$CuFKZP_2W_{18}$ /PPy(15%)	H_2O_2	0.07	5-100	0.0227	**This work**
MOF-808	AA	15	30-1030	0.544	[60]
CuNPs/C	AA	1.41	10-1000	——	[62]
$AgFKZSiW_{12}$ /PPy	AA	2.7	1-80	0.0196	[61]
$CuFKZP_2W_{18}$ /PPy(15%)	AA	0.627	5-100	0.0025	**This work**

Overall mechanism of H_2O_2 and AA colorimetric biosensing

Based on the above experimental result, the proposed mechanism of H_2O_2 and AA colorimetric biosensor on $CuFKZP_2W_{18}$/PPy (n) was speculated shown in Scheme 1. As we all known, PPy can exhibit a strong photo-response and photo-generated hole transporting properties in the visible light regions. Firstly, POMs induces electrons and transfer them to the metal centres through FKZ and PPy from the highest occupied molecular orbital (HOMO) to the lowest unoccupied molecular orbital (LUMO), which can be considered as a parallel process to the band-gap excitation in semiconductor photocatalyst. Secondly, adsorbed H_2O_2 was activated by metal centers through the breaking up of O-O bond coupling with the proton-electron transfer, producing double-active •OH stabilized by $CuFKZP_2W_{18}$/PPy (15%), due to the stronger adsorption capacity of PPy and the consistence of eight helical chains. Thirdly, OPD molecules were adsorbed on the surface of $CuFKZP_2W_{18}$/PPy (15%), donating lone-pair electrons and reacting with desorbed •OH through electron transfer to complete the OPD oxidation and the corresponding color change from colorless to yellow. Finally, When AA is added into the abovementioned system as an inhibitor, oxOPD converts to OPD, meanwhile AA converts to DHAA leading to the fading of yellow color (Scheme S3, SI).

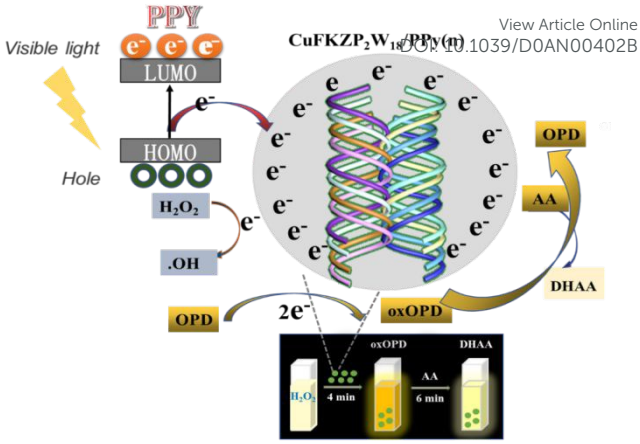

Scheme 1. Proposed mechanistic scheme for the H_2O_2 and AA colorimetric biosensing on $CuFKZP_2W_{18}$/PPy(15%).

Selectivity and Interference assay of AA detection

Considering that other substance in human body may cause interference during the AA detection process, here, Glu, Mg^{2+}, Na^+, Cl^-, NO_3^-, and K^+ ions were selected to assess their inhibitory effects. As shown in Figure 8a, the color and absorption intensity at 422 nm almost remain unchanged when these interferential substances as inhibitors exist in t-he reaction system, expect that the reaction system with AA as inhibitor convert to colorless, namely, the absorption intensity is quenched at 422 nm. This result demonstrates that $CuFKZP_2W_{18}$/PPy(15%) possesses excellent selectivity toward AA colorimetric detection. In addition, to verify the sensing performance for AA in practical applications, the colorimetric detection in pre-mixing potential substances with AA are also studied (Figure 8b). The ΔA value of pre-mixing different potential substances with AA was almost similar to that of AA, indicating that the colorimetric sensor responded specifically towards AA. The relative error of interference effect of potential substances (Glu, Mg^{2+}, Na^+, Cl^-, NO_3^-, and K^+ ions) on AA detection is within the allowable range when it is less than 2.0%, concluding that the proposed $CuFKZP_2W_{18}$/PPy(15%) sensor displays good selectivity to the AA detection in practical applications.

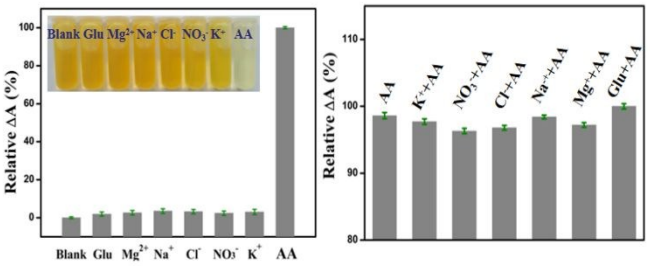

Fig. 8. Selectivity of $CuFKZP_2W_{18}$/PPy(15%) for AA detection. (a) The ΔA422 nm signals of $CuFKZP_2W_{18}$/PPy(15%)-OPD-H_2O_2 sensing system in the presence of 200 μM potential interferences; (b) The ΔA422 nm values of $CuFKZP_2W_{18}$/PPy(15%-OPD-H_2O_2 sensing system in the presence of 80 μM AA and 200 μM potential interferences. Various substances are glucose, Mg^{2+}, Na^+, Cl^-, NO^{3-}, and K^+ and AA (from left to right). All reaction systems contain acetate buffer solution (pH=7), $CuFKZP_2W_{18}$/PPy (0.6 mg/mL), OPD 30 μM, H_2O_2 100 μM and the ΔA422 nm signals were collected is 4 min at 40 °C after initiation.

Determination of AA in human serum samples

View Article Online
DOI: 10.1039/D0AN00402B

Published on 14 April 2020. Downloaded by University of Birmingham on 4/14/2020 9:32:33 AM.

Analyst Accepted Manuscript

View Article Online
DOI: 10.1039/D0AN00402B

To further confirm the reliability of our proposed colorimetric sensor, the detection of AA in serum samples was also performed. The recovery of AA was studied by spiking test samples with four different concentrations. After spiking four groups of standard AA solutions with different concentrations (1, 10, 50 and 100 μM) in 10-fold diluted samples. The results indicate that the recoveries of samples is 99.3-102.5% for human serum samples (Table 4), and the RSDs for five successive measurements were below 5%. The result indicates that the developing AA test method is reliable.

Table 4. Detection of AA in 10% human serum samples.

Samples	AA (μM)*	AA (μM)**	Recovery (%)	RSD (%)
10% Human serum	1	1.03	103	1.47
10% Human serum	10	10.13	101.3	0.96
10% Human serum	50	49.67	99.34	1.13
10% Human serum	100	100.18	100.18	3.26

AA (μM)*= added amounts; AA (μM)**= found amounts.

Reproducibility and Stability evaluation of $CuFKZP_2W_{18}$/PPy (15%)

The repeatability of peroxidase-like mimics is of great significance for practical application of colorimetric sensor. The run experiment of $CuFKZP_2W_{18}$/PPy(15%) as catalyst was performed (Figure S15, SI), and the result shows that the catalytic activity of $CuFKZP_2W_{18}$/PPy(15%) for subsequent three run falls (100% for the first run, 94% for the second run, 86% for the third run) under the same conditions, which may be attributed to the loss of $CuFKZP_2W_{18}$/PPy (15%) during the centrifugation. In addition, PXRD and IR spectra of $CuFKZP_2W_{18}$/PPy(15%) were similar before and after the evaluation of peroxidase-like activity (Figure S16, SI), confirming that $CuFKZP_2W_{18}$/PPy(15%) were very stable as peroxisome-like catalysts and a promising material in biosensing.

Conclusions

In summary, a new Wells-Dawson based crystal compound with eightfold helix ($CuFKZP_2W_{18}$) and its PPy coating composites ($CuFKZP_2W_{18}$/PPy (7%, 15% and 30%)) were successfully prepared, and $CuFKZP_2W_{18}$/PPy (15%) as a new enzyme mimics exhibits excellent peroxidase-like activity and is 3 times higher than that of $CuFKZP_2W_{18}$ using OPD as a colorimetric substrate, owing to the rich active sites, and synergetic effects of components. More importantly, a convenient "on-off switch" colorimetric platform based $CuFKZP_2W_{18}$/PPy (15%) was developed for AA detection with the lowest LOD among all reported enzyme mimics. Moreover, the selectivity and anti-interference performance of $CuFKZP_2W_{18}$/PPy (15%) can also be assured. This method indeed describes a facile and effective route for the fabrication of a highly peroxidase-like mimic in biosensing and medical diagnostics.

Conflicts of interest

There are no conflicts to declare.

Acknowledgements

Financial support from the Talent Culturing Plan for Leading Disciplines and the Natural Science Foundation (ZR2017LB001) of Shandong Province.

References

1 L. Gao, J. Zhuang, L. Nie, J. Zhang, Y. Zhang, N. Gu and X. Yan, *Nat. Nanotechnol.*, 2007, **2**, 577-583.
2 J. M. Perez, *Nat. Nanotechnol*., 2007, **2**, 535-536.
3 H. Wei and E. Wang, *Anal. Chem.*, 2008, **80**, 2250-2254.
4 B. Dalkıran, P. E. Erden and E. Kılıç, *Talanta*, 2017, **167**, 286-295.
5 J. W. Zhang, H. T. Zhang, Z. Y. Du, X. Wang, S. H. Yu and H. L. Jiang, *Chem. Commun.*, 2014, **50**, 1092-1094.
6 X. Jiang, C. Sun, Y. Guo, G. Nie and L. Xu, *Biosens. Bioelectron.*, 2015, **64**, 165-170.
7 S. Song, Y. Qin, Y. He, Q. Huang, C. Fan and H. Y. Chen, *Chem. Soc. Rev*., 2010, **39**, 4234-4243.
8 W. Shi, Q. Wang, Y. Long, Z. Cheng, S. Chen, H. Zheng and Y. Huang, *Chem. Commun.*, 2011, **47**, 6695-6697.
9 X. Qin, Y. Luo, W. Lu, G. Chang, A. M. Asiri, A. O. Al-Youbi and X. Sun, *Electrochim. Acta*, 2012, **79**, 46-51.
10 A. Asati, S. Santra, C. Kaittanis, S. Nath and J. M. Perez, *Angew. Chem.*, 2009, **121**, 2344-2348.
11 J. Chen, Y. Shu, H. Li, Q. Xu and X. Hu, *Talanta*, 2018, **189**, 254-261.
12 Q. Liu, Y. Yang, H. Li, R. Zhu, Q. Shao, S. Yang and J. Xu, *Biosens. Bioelectron.*, 2015, **64**, 147-153.
13 Y. Song, K. Qu, C. Zhao, J. Ren and X. Qu, *Adv. Mater*., 2010, **22**, 2206-2210.
14 W. Haider, A. Hayat, Y. Raza, A. A. Chaudhry and J. L. Marty, *RSC Adv.*, 2015, **5**, 24853-24858.
15 Y. Tao, E. Ju, J. Ren and X. Qu, *Chem. Commun.*, 2014, **50**, 3030-3032.
16 A. Olgun, A. T. Çolak, İ. H. Gübbük, O. Şahin and E. Kanar, *J. Mol. Struct.*, 2017, **1134**, 78-84.
17 J. J. Walsh, A. M. Bond, R. J. Forster and T. E. Keyes, *Coordin. Chem. Rev*., 2016, **306**, 217-234.
18 C. L. Hill, *Chem. Rev*., 1998, **98**, 1-2.
19 Z. Fu, W. Gao, T. Yu and L. Bi, *Talanta*, 2019, **195**, 463-471.
20 J. C. Liu, Q. Han, L. J. Chen, J. W. Zhao, C. Streb and Y. F. Song, *Angew. Chem. Int. Ed.,* 2018, **57**, 8416-8420.
21 Y. Zhang, Y. M. Li, J. J. Pang, Y. F. Liu, P. Li, L. J. Chen and J. W. Zhao, *Inorg. Chem.*, 2019, **58**, 7078-7090.
22 J. Wang, D. Han, X. Wang, B. Qi and M. Zhao, *Biosens. Bioelectron.*, 2012, **36**, 18-21.
23 S. Liu, J. Tian, L. Wang, Y. Zhang, Y. Luo, H. Li and X. Sun, *ChemPlusChem.*, 2012, **77**, 541-544.
24 D. Li, H. Han, Y. Wang, X. Wang and Y. Li, E. Wang, *Eur. J. Inorg. Chem.*, 2013, **10-11**, 1926-1934.
25 F. J. Ma, S. X. Liu, C. Y. Sun, D. D. Liang, G. J. Ren, F. Wei and Z. M. Su, *J. Am. Chem. Soc.*, 2011, **133**, 4178-4181.
26 W. Zhang, G. Jia, Z. Li, C. Yuan, Y. Bai and D. Fu, *ADV. Mater. Interfaces*, 2017, **4**, 1601241.
27 R. Yu, X. F. Kuang, X. Y. Wu, C. Z. Lu and J. P. Donahue, *Coord. Chem. Rev.*, 2009, **253**, 2872-2890.
28 D. Y. Du, J. S. Qin, S. L. Li, Z. M. Su and Y. Q. Lan, *Chem. Soc. Rev.*, 2014, **43**, 4615-4632.
29 S. Li, L. Zhang, Y. Lan, K. P. O' Halloran and H. Ma, H. Pang, *Chem. Comm.*, 2018, **54**, 1964-1967.
30 F. Xie, X. Li, Y. Li, X. Jiang, Q. Rui and J. Sha, *J. Coord. Chem.*, 2019, **72**, 272-282.
31 J. Q. Sha, X. Y. Yang, Y. Chen, P. P. Zhu, Y. F. Song and J. Jiang, *ACS Appl. Mater. Interfaces*, 2018, **10**, 16660-16665.
32 X. Yang, P. Zhu, J. Ren, Y. Chen, X. Li, J. Sha and J. Jiang, *Chem. Comm.*, 2019, **55**, 1201-1204.

Published on 14 April 2020. Downloaded by University of Birmingham on 4/14/2020 9:32:33 AM.

Analyst Accepted Manuscript

This journal is © The Royal Society of Chemistry 20xx

Please do not adjust margins

View Article Online
DOI: 10.1039/D0AN00402B

Published on 14 April 2020. Downloaded by University of Birmingham on 4/14/2020 9:32:33 AM.

33 Y. Ma, H. Peng, J. Liu, Y. Wang, X. Hao, X. Feng, S.U. Khan, H. Tan and Y. Li, *Inorg. Chem.*, 2018, **57**, 4109-4116.
34 C. Y. Sun, S. X. Liu, D. D. Liang, K. Z. Shao, Y. H. Ren and Z. M. Su, *J. Am. Chem. Soc.*, 2009, **131**, 1883-1888.
35 C. T. Buru, P. Li, B. L. Mehdi, A. Dohnalkova, A. E. Platero-Prats, N. D. Browning, K. W. Chapman, J. T. Hupp and O. K. Farha, *Chem. Mater.*, 2017, **29**, 5174-5181.
36 T. Nakano, Y. Okamoto and *Chem. Rev.*, 2001, **101**, 4013-4038.
37 M. T. Li, L. N. Cong, J. Zhao, T. T. Zheng, R. Tian, J. Q. Sha, Z. M. Su and X. L. Wang, *J. Mater. Chem. A*, 2017, **5**, 3371-3376.
38 X. Y. Yang, M. T. Li, N. Sheng, J. S. Li, G. D. Liu, J. Q. Sha and J. Z. Jiang, *Cryst. Growth Des*., 2018, **18**, 5564-5572.
39 P. P. Zhu, L. J. Sun, N. Sheng, J. Q. Sha, G. D. Liu, L. Yu, H. B. Qiu and S. X. Li, *Cryst. Growth Des.*, 2016, **16**, 3215-3223.
40 Z. Ma, Y. Qiu, H. Yang, Y. Huang, J. Liu, Y. Lu and P. Hu, *ACS Appl. Mater. Interfaces*, 2015, **7**, 22036-22045.
41 X. Li, X. Y. Yang, J. Q. Sha, T. Han, C. J. Du, Y. J. Sun and Y. Q. Lan, *ACS Appl. Mater. Interfaces*, 2019, **11**, 16896-16904.
42 L. J. Farrugia, *J. Appl. Crystallogr.*, 2012, **45**, 849-854.
43 Y. Jiao, G. Chen, D. Chen, J. Pei and Y. Hu, *J. Mater. Chem. A,* 2017, **5** 23744-23752.
44 X. Jian, H. M. Yang, J. G. Li, E. H. Zhang, L. L. Cao and Z. H. Liang, *Electrochim. Acta,* 2017, **228**, 483-493.
45 Y. Jia, S. Sun, X. Cui, X. Wang and L. Yang, *Talanta*, 2019, **205**, 120139.
46 J. Q. Sha, X. Y. Yang, N. Sheng, G. D. Liu, J. S. Li and J. B. Yang, *J. Solid State Chem.*, 2018, **263**, 52-59.
47 W. Q. Kan, J. Yang, Y. Y. Liu and J. F. Ma, *Inorg. Chem.*, 2012, **51**, 11266-11278.
48 X. Liu, Q. Wang, H. Zhao, L. Zhang, Y. Su and Y. Lv, *Analyst*, 2012, **137**, 4552-4558.
49 D.F. Chai, Z. Ma, H. Yan, Y.F. Qiu, H. Liu, H.D. Guo and G.G. Gao. *RSC Adv.*, 2015, **5**, 78771-78779.
50 H. Yang, R. Yang, P. Zhang, Y. Qin, T. Chen and F. Ye, *Microchim. Acta* 2017, **184**, 4629-4635.
51 Y. L. Liu, X. J. Zhao, X. X. Yang and Y. F. Li, *Analyst*, 2013, **138**, 4526-4531.
52 L. Ai, L. Li, C. Zhang, J. Fu and J. Jiang, *Chem. Eur. J.*, 2013, **19**, 15105-15108.
53 M. C. Kim and S. Y. Lee, *Nanoscale*, 2015, **7**, 17063-17070.
54 D. J. Porter and H. J. Bright, *J. Biol. Chem.*, 1983, **258**, 9913-9924.
55 T. Zhang and Y. Lu, G. Luo, *ACS Appl. Mater. Interfaces,* 2014, **6**, 14433-14438.
56 J. Lu, H. Zhang, S. Li, S. Guo, Li Shen, T. Zhou and Y. Zhang, *Inorg. chem*., 2020, **59**, 3152-3159.
57 Y. Jv, B. Li, R and Cao, *Chem. Commun.*, 2010, **46**, 8017-8019.
58 J. Sun, C. Li and Y. Qi, *Sensors*, 2016, **16**, 584-595.
59 H. Zhao, Y. Dong and P. Jiang, *ACS Appl. Mater. Interfaces*, 2015, **7**, 6451-6461.
60 H. Q. Zheng, C. Y. Liu, X. Y. Zeng, J. Chen, J. Lü, R. G. Lin and J. W. Su, *Inorg. chem.*, 2018, **57**, 9096-9104.
61 X. Li, L. Sun, X. Yang, K. Zhou, G. Zhang, Z. Tong and J. Sha, *Analyst*, 2019, **144**, 3347-3356.
62 H. Tan, C. Ma, L. Gao, Q. Li, Y. Song, F. Xu and L. Wang, *Chem. Eur. J.*, 2014, **20**, 16377-16383.

Analyst Accepted Manuscript

Please do not adjust margins

View Article Online
DOI: 10.1039/D0AN00402B

Table of Contents

Polypyrrole Coating Eightfold Helical Wells-Dawson POMs based Cu-FKZ Framework for Boosting Colorimetric Sensing

Qian Li,[a,b] Mingqi Xu,[a,b] Xiao Li,[a] Shuxian Li,[b] Liran Hou,[a] Yuhao Chen,[a] Jingquan Sha*[a,b]

[a] Department of Chemistry and Chemical Engineering, Jining University, Qufu 273155, P. R. China

[b] School of Pharmacy, Jiamusi University, HeilongJiang, Jiamusi, 154007, P.R. China

*Corresponding author: E-mail address: shajq2002@126.com.

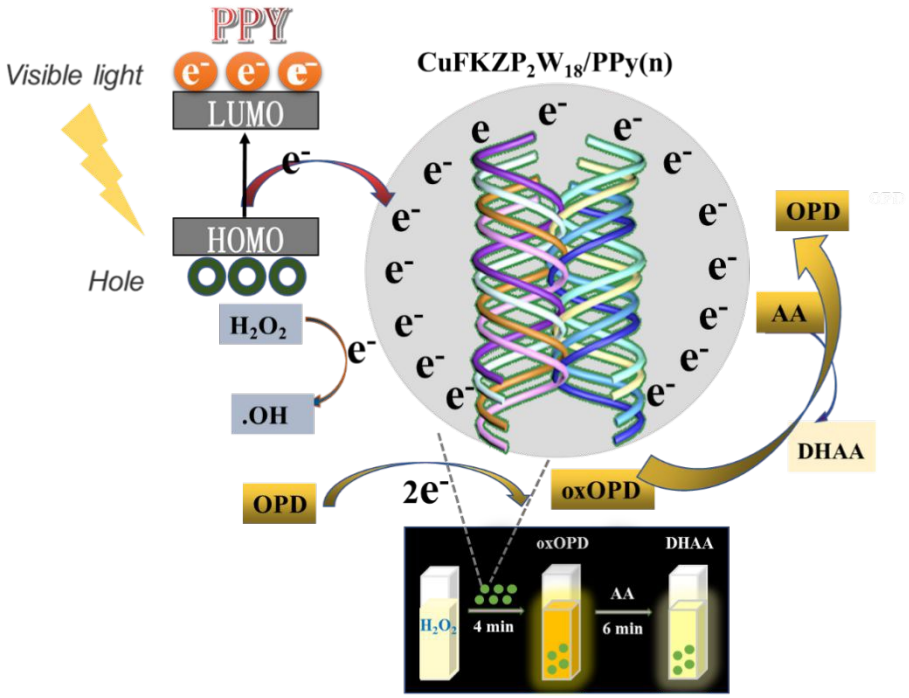

A new Wells-Dawson type $CuFKZP_2W_{18}$ based hybrid compound containing eightfold helical chains is reported, and its $CuFKZP_2W_{18}$/PPy(15%) composite exhibits excellent peroxidase-like catalytic activities.

Published on 14 April 2020. Downloaded by University of Birmingham on 4/14/2020 9:32:33 AM.

Analyst Accepted Manuscript